Journal of Applied Mathematics and Physics, 2020, 8, 710-726
https://www.scirp.org/journal/jamp
ISSN Online: 2327-4379
ISSN Print: 2327-4352

Phase Transition (Spinel-Ortho) Ferrite Doped with Holmium

M. M. Elsehly[1], D. M. Hemeda[2], O. M. Hemeda[2], H. M. Alabany[2], B. I. Salem[2*]

[1]Physics Department, Common First Year, Umm Al-Qura University, Mecca, KSA
[2]Physics Department, Faculty of Science, Tanta University, Tanta, Egypt
Email: *basant.salem@science.tanta.edu.eg

How to cite this paper: Elsehly, M.M., Hemeda, D.M., Hemeda, O.M., Alabany, H.M. and Salem, B.I. (2020) Phase Transition (Spinel-Ortho) Ferrite Doped with Holmium. *Journal of Applied Mathematics and Physics*, **8**, 710-726.
https://doi.org/10.4236/jamp.2020.84055

Received: January 24, 2020
Accepted: April 18, 2020
Published: April 21, 2020

Abstract

A series of perovskite type oxides with formula $La_{1-x}Ho_xFeO_3$, with Ho substitute for La, where (x = 0.1, 0.2, 0.3 and 0.4). The samples have been prepared by the standard ceramic technique, sintered at 1200˚C for nine hours. Their crystalline structure was investigated using X-ray diffraction and IR spectroscopy. The X-ray diffraction analysis illustrates that the system $La_{1-x}Ho_xFeO_3$ has a perovskite orthorhombic phase. IR absorption spectra of $La_{1-x}Ho_xFeO_3$ showed two main characteristic absorption bands in the far infrared region. These bands are assigned to oxygen octahedral bending vibration and oxygen tetrahedron stretching vibration. It was found that the DC electrical conductivity increases linearly with temperature ensuring the semiconducting nature of the samples. The dielectric properties, Electron Spin Resonance (ESR) spectra, and thermal properties have been studied, to go through the material and explore its ability to be used for many industrial applications.

Keywords

Lanthanum Holmium Ferrite, Perovskite, Ceramic, XRD, ESR Spectra, DC Resistivity

1. Introduction

Ferrites have a paramount advantage over other types of magnetic materials, high electrical resistivity and resultant low eddy current losses over wide range. These materials are important in microwave components such as circulators and phase shifters. In some cases, the ferrite must act as a microwave field attenuator or absorb an incoming microwave signal. The most important application of ferrites is as square loop memory cores in computers. Semiconducting magnetic

oxides are widely used as thermistors. At present, there is much interest in devices based on magneto-optical phenomena, especially the Faraday effect in garnet [1]. High permeability ferrites find important applications in increasing the recording efficiency of magnetic heads stopples [2]. The densities of ferrites are significantly lower than those of their thin metal counterparts; thus a component of the same size would be lighter in ferrite.

The thermal conductivity of ferrites is rather low. This feature becomes quite important in its application in power transformers where the considerable heat generated is not easily lost. Thus, the center of a core will accumulate the heat, and possibly exceeding the Curie point, the thermal conductivity of ferrites is in the range of $(10 - 15) \times 10^{-3}$ cal /sec·cm·˚C.

The rare-earth orthoferrites of the formula $RFeO_3$, where R is a trivalent rare-earth ion, were first identified in 1950 by Forestier and Guit-Guillain [3] who also characterized their magnetic properties. They form an important series for magnetic studies and have been extensively studied, in the sixties and seventies both in polycrystalline and single crystalline form. The orthoferrite crystals in the first approximation are treated as perovskites but the true symmetry is orthorhombic, with the c-axis forming one of the pseudo axes. The angle between the c-axis and the a-b plane is 90.6 [4]. A previous study on orthoferrites is done and this article considered as a review on the magnetic and spectroscopic properties of the rare earth ortho-ferrite (Ho ortho-ferrite and different types). The paper deals with some experimental studies as spin structure, magnetic symmetry in orthoferrite. It also studied the spin reorientation transition, the magnetic ordering at low temperature 2˚K - 6˚K, spectroscopy exchange interaction, domain wall and hysteresis loop [5].

2. Materials and Methods

Solid solution of the system $La_{1-x}Ho_xFeO_3$ (x = 0.0, 0.1, 0.2, 0.3 and 0.4) was prepared using a double sintering ceramic technique [6] [7]. The pure stoichiometric oxide Fe_2O_3 and rare earth element oxides (Ho_2O_3) were weighted with molecular weight ratio, then the used oxides (powder) were mixed together. The mixture was ground in order to obtain a very fine powder. Then mixtures were pre-sintered at 950˚C for eight hours and slowly cooled to room temperature.

The fine powder was pressed at room temperature and pressure of 10 Kp/cm^2 into the form of discs of diameter (1.3 cm) and triodes, samples were then finally sintered to 1200˚C for nine hours under the normal conditions of atmospheric pressure and slowly cooled to room temperature. A Flow chart of sample preparation stages is shown in **Figure 1**.

X-ray diffraction pattern was performed by using Shimadzu X-ray powder diffractometer. Infrared spectra for the prepared samples were carried out at room temperature by using a PERKIN-ELMER-1430 spectrometer where the infrared spectra are recorded in the range 200 to 1500 cm^{-1}. The ESR spectra were recorded for the samples using JES-FE2xG Joel ESR spectrometer. The DC

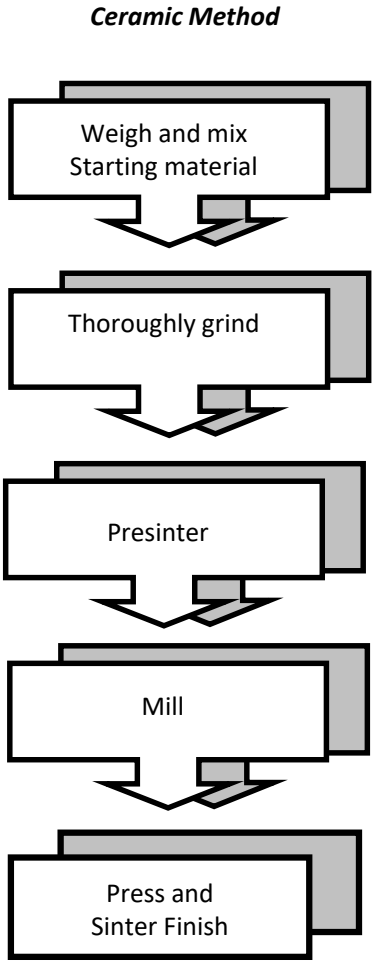

Figure 1. Flow chart of sample preparation stages.

resistivity was measured using an electrometer (type Keithely 610C) as shown in **Figure 2**.

3. Result and Discussion

3.1. X-Ray Diffraction Analysis

The X-ray diffraction analysis of $La_{1-x}Ho_xFeO_3$ where (x = 0.0, 0.1, 0.2, 0.3 and 0.4) indicates that all the samples have an orthorhombic structure as shown in **Figure 3**. The diffraction peaks were shifted as the Ho content increases. Lattice parameter a, b and c, and the unit cell volume are listed in **Table 1**. The results indicate that the structure of the compound is similar to that of $RFeO_3$ as reported by Geller and Wood [8].

The structure of $RFeO_3$ (where R means La and Ho ions at A site) is not ideal perovskite and the Fe^{3+} ions and O^{2-} ions depart from the ideal positions due to the difference between the radius of R ions and the Fe ions. In $La_{1-x}Ho_xFeO_3$ ferrite the distortion will be larger because there are two kinds of large ions, La and Ho ions at R site. In accordance to the literature data the material transfer to the orthoferrite system [8].

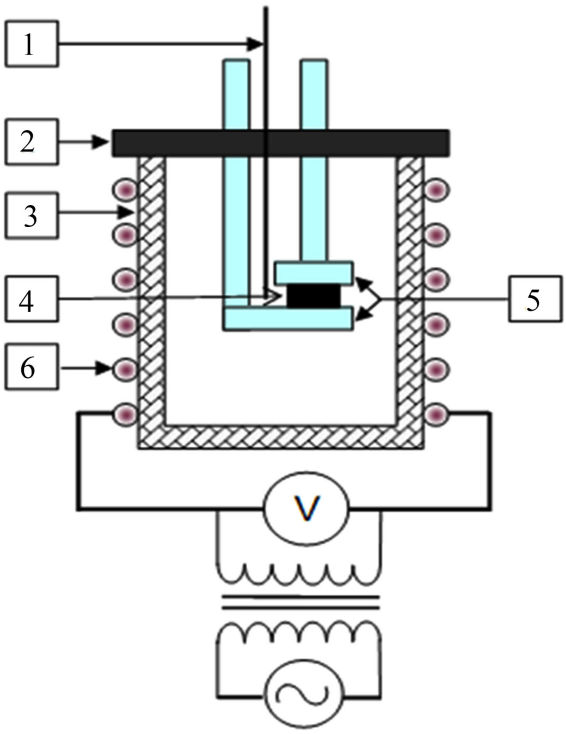

Figure 2. The DC resistivity cell. 1-Digital thermometer; 2-Cover; 3-Shield; 4-Sample; 5-Two electrodes; 6-Heater.

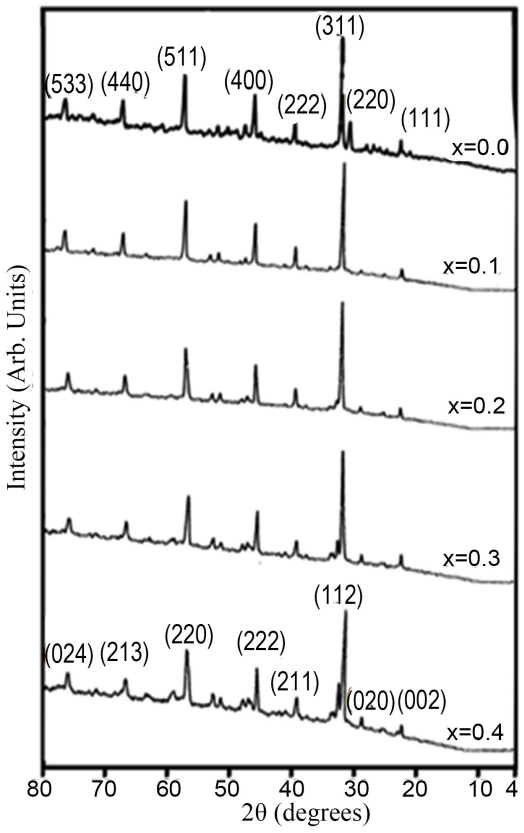

Figure 3. XRD of $La_{1-x}Ho_xFeO_3$ with $x = 0.0, 0.1, 0.2, 0.3$ and 0.4.

Table 1. The lattice parameters (*a*, *b* and *c*), volume of the lattice, tolerance factor *t* and the ratio *c*/*a* as a function of composition of the system $La_{1-x}Ho_xFeO_3$ ferrite.

x	Compound	*a* (Å)	*B* (Å)	*C* (Å)	*V* (Å^3)	*t*	r_A (Å)	r_B (Å)	*c*/*a*
0.0	$LaFeO_3$	5.192	5.62	7.86	229.34	0.91	0.82	0.33	1.51
0.1	$La_{0.9}Ho_{0.1}FeO_3$	5.057	5.59	7.23	204.71	0.85	0.738	0.37	1.42
0.2	$La_{0.8}Ho_{0.2}FeO_3$	5.409	5.51	7.37	219.84	0.80	0.656	0.42	1.36
0.3	$La_{0.7}Ho_{0.3}FeO_3$	5.442	5.49	7.31	218.53	0.75	0.574	0.46	1.34
0.4	$La_{0.6}Ho_{0.4}FeO_3$	5.282	5.46	7.34	212.03	0.70	0.492	0.50	1.39

A larger ion occupies A positions with coordination number 12 and Fe^{3+} ions occupy B with coordination number 6. Accordingly, the La^{3+} ions and Ho occupy the A position. The requirement of stability of this orthoferrites is that the Goldschmidt tolerance factor should be nearly unity [9]. The tolerance factor (*t*) is given by the following equation:

$$t = \frac{r_A + r_o}{\sqrt{2}\left(r_B + r_o\right)}$$

where r_A, r_B and r_o are the ionic radii of the A- and B-site ions and the O^{2-} ion, respectively.

From Table 1, the values of lattice parameters *a* and *b* approximately equal $c/\sqrt{2}$. The volume of the unit cell increases with increasing Ho content because the radius of Ho = 0.86 Å is larger than La = 0.82 Å. The values of the lattice parameters *a*, *b* and *c* are near that of La FeO_3 which has the values *a* = 5.53 Å, *b* = 5.57 Å, *c* = 7.8 Å and *V* = 241 Å^3. The tolerance factor (*t*) as given in Table 1 decreases and ranges from 0.91 to 0.70 indicating that the lattice is distorted slightly by the addition of Ho^{3+} ions. The substitution of Ho^{3+} ions for La^{3+} ions causes *c*/*a* to decrease as shown in Table 1. The replacement of La^{3+} by Ho^{3+} at A sites may reduce the covalent bond formation by La^{3+} ions thereby decreasing the lattice parameter *c* and increase *a*.

The stability of the perovskite structure decreases by increase Ho ion as the tolerance factor decrease as given in Table 1. The density of the samples increases up to *x* = 0.2 and slowly decreases with increasing Ho content. The theoretical density D_x is greater than the bulk density due to the presence of pores in the material. The orthorhombic phase resists the movement of grain boundaries and prevents the grain growth leading to increase in the number of inner pores giving rise to the density as shown in Figure 4.

The crystallite size of BST was calculated using Scherer's equation [10]:

$$d = \frac{k\lambda}{\beta\cos\theta}$$

where k = 0.89 is constant, θ is the peak location, β is the full width at half maximum of the peak, and λ is the wavelength of the X-ray for Cu-Kα radiation (λ = 1.540598 Å). The behavior of crystallite size is shown in Figure 5. It was

observed that the crystallite size tends to decrease with increasing Ho content. This is because Ho ions inhibit grain growth during sintering process leading to decrease of crystallite size.

The lattice parameters of $La_{1-x}Ho_xFeO_3$ were similar to that given by standard orthorhombic ferrite in literature as shown in Figure 6.

Figure 7 shows the relation between r_A and r_B for $La_{1-x}Ho_xFeO_3$ as a function of Ho content. The radius of the tetrahedral site r_A decreases and r_B increases.

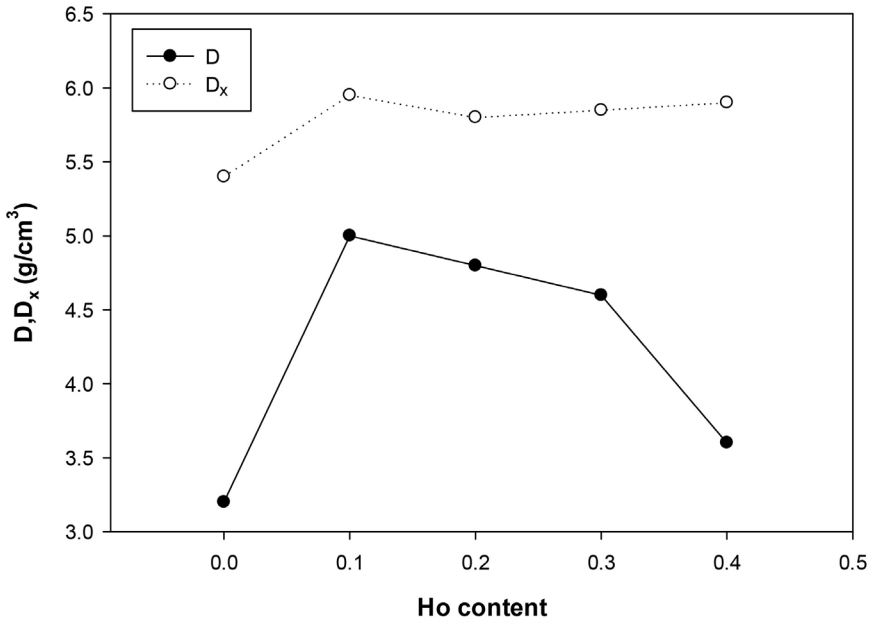

Figure 4. The relation between the experimental density (D), theoretical density (D_x) and Ho content.

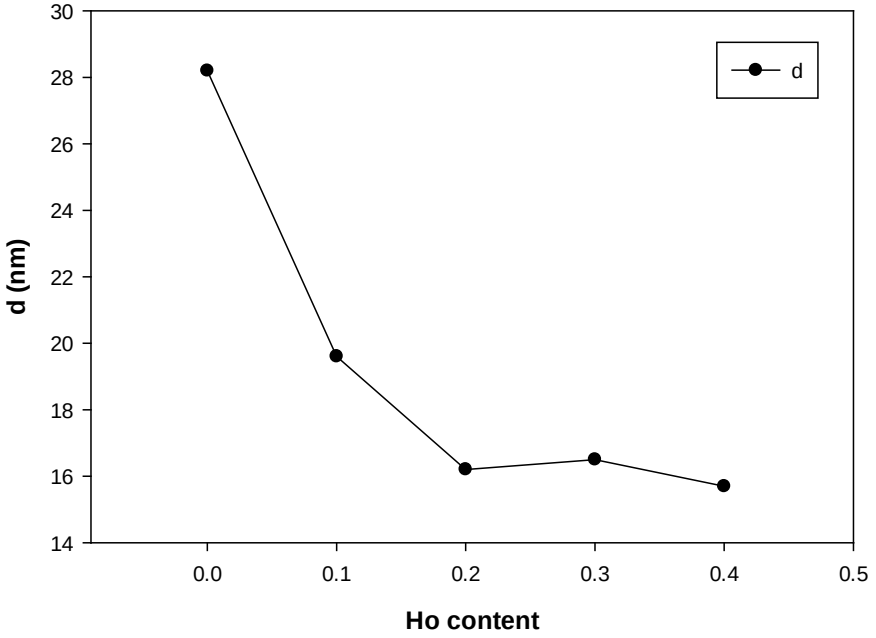

Figure 5. The relation between the crystallite size (d) and Ho (content).

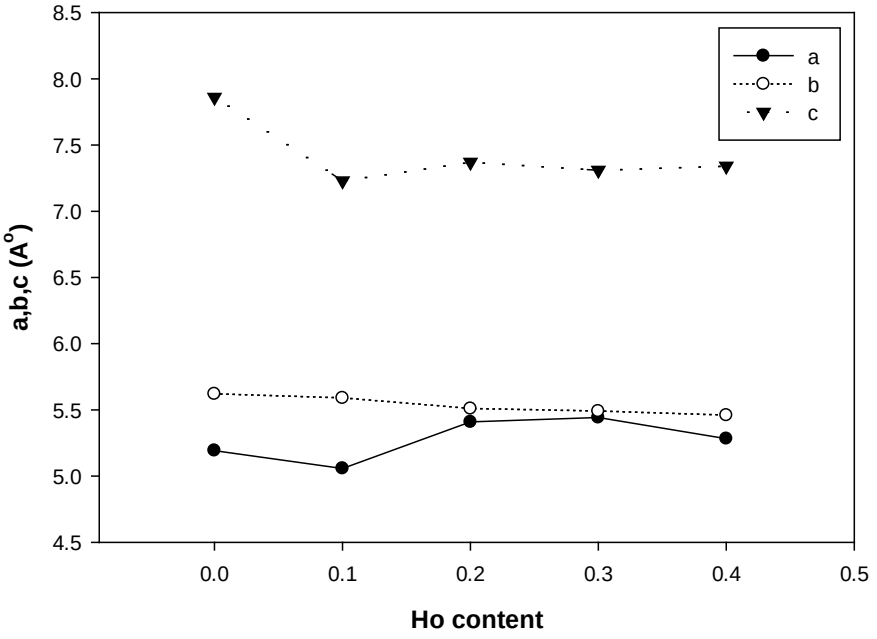

Figure 6. The relation between the lattice parameters (*a*, *b*, and *c*) and Ho content.

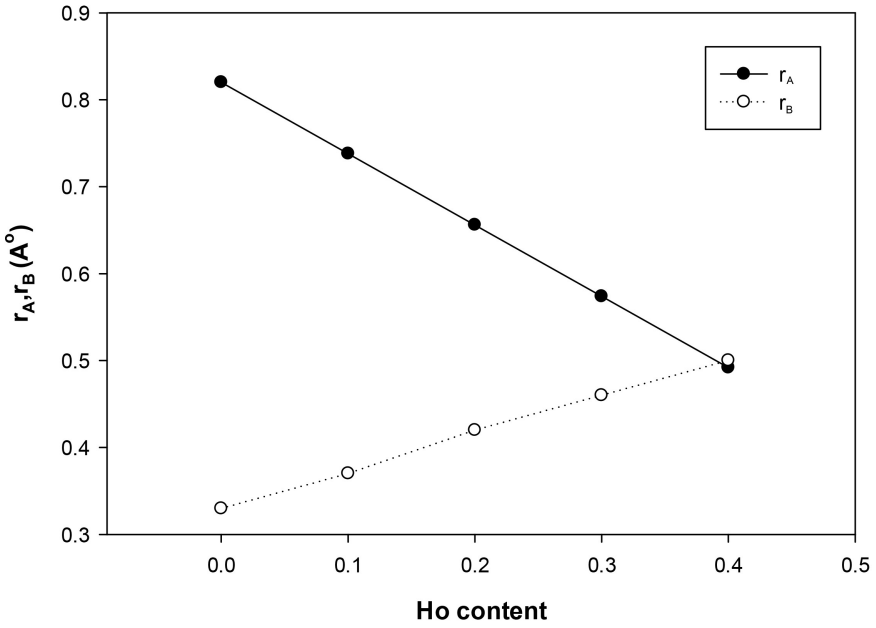

Figure 7. The relation between the tetrahedral radius (r_A), octahedral radius (r_B) and Ho content.

The substitution of Ho^{3+} ions with radius 0.86 Å at A site increases r_A. The migration of Fe^{3+} from B site as *a* of A site expansion causes a decrease of r_B values.

3.2. FTIR Spectra

The IR spectra in a wide range of wavenumber (200 - 1500 cm^{-1}) was carried out for $La_{1-x}Ho_xFeO_3$ for (x = 0.0, 0.1, 0.2, 0.3, and 0.4) as shown in **Figure 8**. The IR spectra show the presence of two characteristic absorption bands in the far

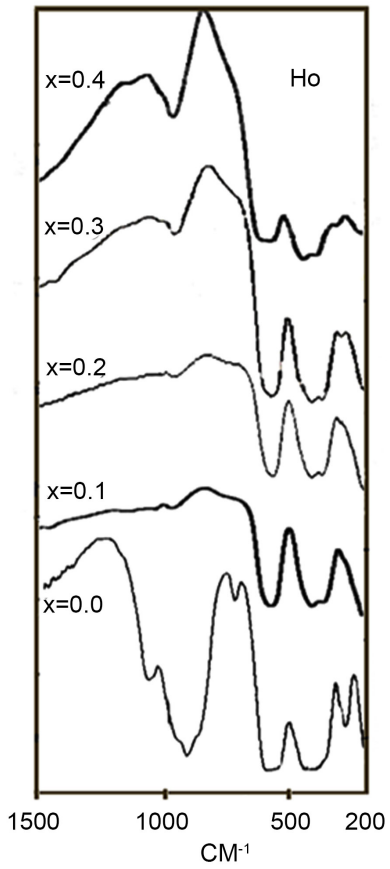

Figure 8. FTIR spectra of $La_{1-x}Ho_xFeO_3$ ferrite.

infrared region. The lower frequency band assigned to oxygen octahedral O-Fe-O bending vibration [11] whereas the higher frequency absorption band assigned to oxygen tetrahedron Fe-O stretching vibration. The other weak bands appeared near lower frequency absorption band, which was resulted from the vibration of La^{3+}-O^{2-} bond, which decrease by increasing Ho content [12].

The spectra of the entire ferrite sample have been used to locate the band positions and are given in **Table 2**. The lower frequency absorption band ν_2 shifted to higher frequency as Hocontent increases and ν_1 shift to lower frequency. The broadening of the spectral band is due to statistical distribution of cation over A and B positions.

The vibration frequency depends on the cation mass, cation-oxygen distance. The change in the lattice constant and bond length are responsible for this shift of the frequency. The shift in ν_1 from 575 to 556 cm^{-1} is due to the change of A ions positions which probably causes the oxygen ions to shift towards the Ho ions.

Splitting occurred at the ν_2 absorption band which is assigned to the formation of Fe^{2+} and confirms our discussion for explanation the conduction mechanism of our studied samples. It has been shown previously that the presence of Fe^{2+} ions at A sites can produce splitting in the IR absorption band. This is attributed to Jahn-Teller distortion produced by Fe^{2+} ions which produces local

Table 2. The variation of wave number of IR absorption peak with x content.

(x)	ν_1 (cm^{-1})	I_{ab}	ν_2 (cm^{-1})	I_{ab}	ν_3 (cm^{-1})	I_{ab}	ν_4 (cm^{-1})	I_{ab}
0.0	405	3.4	575	3.2	288	14.2	-	-
0.1	413	14.8	567	14.9	-	-	-	-
0.2	411	6.8	562	7.1	-	-	296	Sholder
0.3	412	3.3	559	3.4	368	3.4	296	28.1
0.4	433	3.7	556	3.2	-	-	296	9.2

deformation in the crystal potential field and hence leads to the splitting of the absorption band.

The small band appears at 296 cm^{-1} for the samples $x = 0.3$ and 0.4 and as a shoulder for $x = 0.2$ and which assigned as υ_4 may be attributed to the Ho^{3+}-O^{2-} bond vibration. This absorption band does not appear for the sample $x = 0.0$ and 0.1. From the IR spectra it can be noticed that the intensity of both two characteristic bands υ_1 and υ_2 decreases as Hocontent increases. It is known that the intensity ratio is a function of the change in dipole moment with intermolecular distance $d\mu/dr$ [13]. This value represents the contribution of Fe-O bond to the dipole moment, so the IR spectra give an idea about the change of molecular structure of ferrite due to the change in Fe-O bond by introducing Ho ions.

The calculated values of force constant are shown in **Figure 9** as a function of Ho content and given from the following equation:

$$F = 4\pi^2 C^2 \mu \nu^2$$

where C is the velocity of light in (cm/sec), ν is the wavenumber and μ is the reduced mass of Fe^{3+} and O^{2-} ions and F_1 and F_2 are the force constants for A and B sites respectively.

There is a correlation between the structure and the geometry of the exchange bond, especially the angle and length of this chemical bond. The decrease in the bond angle Fe-O-Fe results in a weaker overlap between Fe 3d and O 2p shells and hence small negative charge on the oxygen atom which reduce the oxygen energy level. On the other hand, the electronic distribution of Fe-O is greatly affected when Ho ions with $4f^4\ 5d^6\ 6s^2$ orbitals are introduced in its neighborhood and affect ($d\mu/dr$) of the Fe-O bond leading to the change of vibration frequency as shown in the IR absorption spectra.

3.3. DC Resistivity

It is known that the rare earth ferrites are a good electrical insulator and have resistivity at room temperature greater than 10^6 Ω·cm [14]. **Figure 10** shows the plot of Lnρ as a function of inverse temperature for the samples $La_{1-x}Ho_xFeO_3$, x = (0.0, 0.1, 0.2, 0.3 and 0.4). The resistivity decreases with increasing temperature.

Also, one can distinguish two regions of different activation energies. The change in the slope of these lines takes place around the Curie temperature T_C which is indexed in **Table 3**. The values of T_c in our studied ferrite ranged from

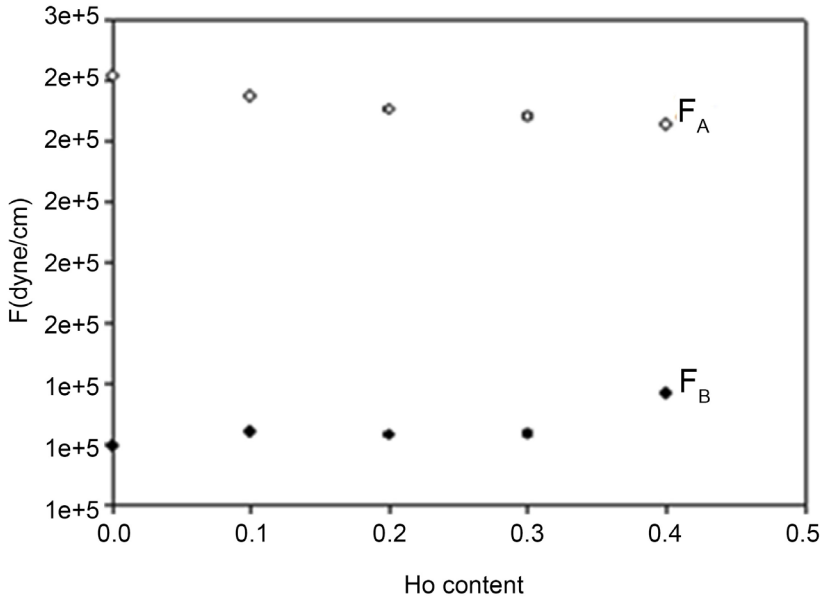

Figure 9. The force constant as a function of Ho content.

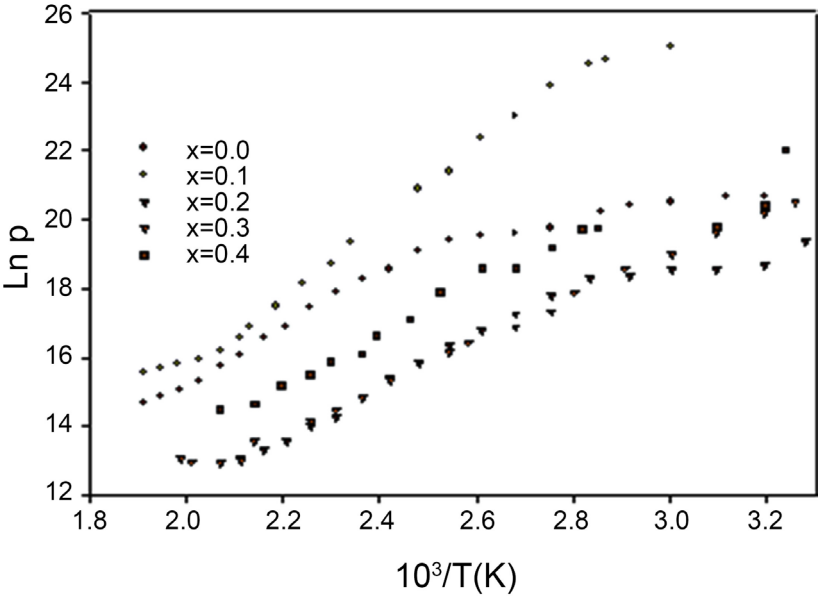

Figure 10. The relation between DC resistivity of $La_{1-x}Ho_xFeO_3$ and 1000/*T*.

Table 3. Effect of composition on phase transition temperature and activation energy of the system $La_{1-x}Ho_xFeO_3$ ferrite.

X_{Ho}	T_C	E_σ			$E_{\sigma T}$			$E_{hop.}$ / E_a	E_{ex} / kT_c	$E_\alpha\alpha$	$T_C(a)$	E_μ
		E_f	E_p	E_f-E_p	E_f	E_p	E_f-E_p					
0.0	140	0.18	0.70	0.52	0.22	0.74	0.51	0.04	0.012	$5.02e^{-6}$	144	0.22
0. 1	127	0.87	1.00	0.12	0.91	1.06	0.15	0.03	0.011	$1.80e^{-4}$	145	0.92
0. 2	171	0.09	0.60	0.51	0.12	0.62	0.50	0.02	0.014	$4.77e^{-5}$	176	0.16
0. 3	72	0.47	0.57	0.09	0.49	0.58	0.08	0.01	0.006	$1.16e^{-4}$	81	0.46
0. 4	113	0.30	0.71	0.40	0.31	0.62	0.30	0.013	0.009	$1.78e^{-4}$	116	0.33

(413 - 345 K) which is near the value given previously [15]. All the curves can be described by the equation:

$$\rho = A_1 \exp\left(\frac{E_f}{kT}\right) + A_2 \exp\left(\frac{E_\rho}{kT}\right)$$

where E_f and E_p are the activation energies below and above the T_c. The samples containing Ho have lower resistivity than $LaFeO_3$. The resistivity decreases by increasing Ho content due to the formation of Fe^{2+} after Ho doping as illustrated in IR section, that will participate in the conduction process and decreases the resistivity [16].

Table 3 gives the activation energies in the two regions as a function of Ho content. The region below T_c is characterized by low activation energy of all samples which strongly suggest the conduction mechanism in the given ferrite formed by hopping electron between Fe^{2+} and Fe^{3+} at A site. In this temperature interval the activation energies values vary from 0.87 to 0.09 eV. The jump in the activation energy ΔE equals to $E_p - E_f$ was obtained for all samples. The ΔE jump is smaller for Ho content. The large slopes of the straight lines at higher temperatures can be regarded as due to thermally activated mobility of charge carriers and not to generation of new charge carriers. This would provide a simple explanation for the low resistivity at high temperature. The resistivity decreases gradually from room temperature to the T_C temperature with an abrupt change at T_C due to the transition from ferrimagnetic to paramagnetic state.

3.4. ESR Spectra

The first derivative ESR spectra of the given ferrite $La_{1-x}Ho_xFeO_3$ are shown in Figure 11, these spectra were converted to absorption spectra which were used to estimate the line width ΔH and the resonance field H_r.

Absorbed microwave power by the ferrite in arbitrary unit as a function of magnetic field is shown in Figure 12.

The line shape of the ESR spectra has a maximum value at a resonance field H_r. The line shape of the ESR spectra for the first sample was found to have nearly Lorentzian shape. For $x = 0.2$, 0.3 and 0.4 The ESR spectra deviate from Lorentzian shape and hyperfine interaction takes place between the first spinel phase (La ferrite) and the second orthorhombic phase (La Ho ferrite) and two peaks appear. The X-ray diffraction patterns of $La_{1-x}Ho_xFeO_3$ indicate that all samples possess an orthorhombic structure.

As given in literature, the porosity increased by Ho addition [17] [18]. The decreased of H_r for the orthorhombic phase from 3590 to 2250 Gauss may be due to the increase of porosity. The line width changes from 1000 to 1363 Gauss by Ho addition. For instance, the dielectric loss of ferrites at microwave frequency largely depends on their ESR line width. For increasing the line width of broadening ΔH, the electric energy loss in the sample also increases. We can conclude from the above discussion that different composition with Ho addition has higher ΔH values and exhibit high loss than the sample without Ho content.

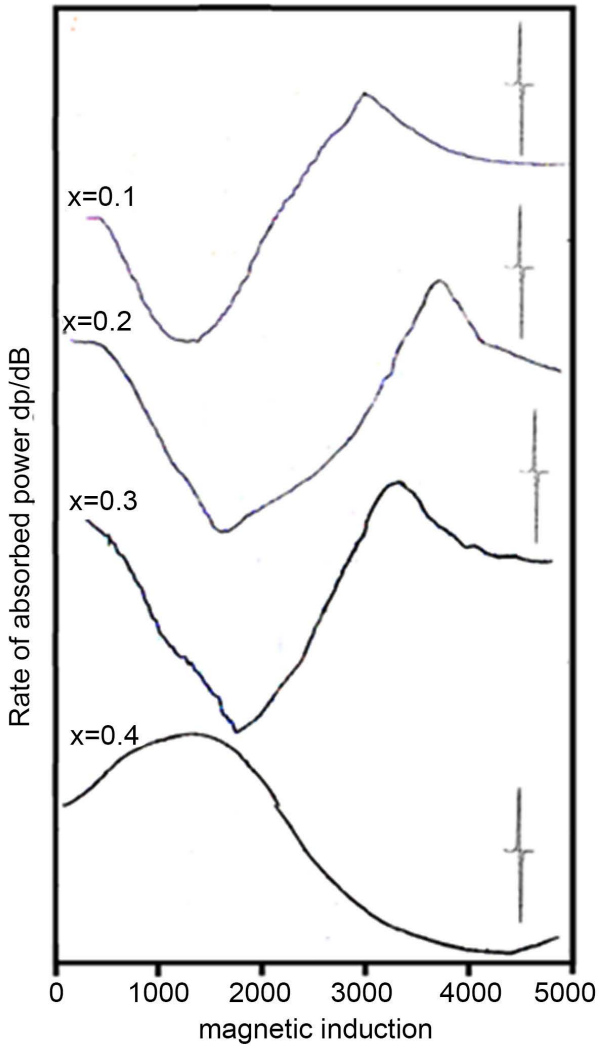

Figure 11. ESR spectra for the system $La_{1-x}Ho_xFeO_3$ ferrite.

This is very important in the application for manufacturing the materials which is used as cores of transformers in microwave region.

The spectroscopic splitting factor g for the samples was calculated and is given in **Table 4**. They have completely different values from the value of free electron (2.0023). Byeon and Hong studied the effect of Fe^{2+} concentration in Mn-Zn ferrite on the line width of the ESR spectra [19]. They attributed the increase of the line width to the increase of Fe^{2+} concentration. In the present study the concentration of Fe^{2+} increase with Ho content as obtained from the IR analysis of the given ferrite, which is accompanied by the increase in the ESR line width. This is in agreement with the study of Galt-Clogston [20] [21] which state that the presence of Fe^{2+} ions at octahedral site can cause broadening of the line width.

The spin lattice relaxation process τ is characterized by time constant which is a function of static magnetic field and depends on the rate at which microwave energy can be absorbed and dissipated. The relaxation time is correlated with the

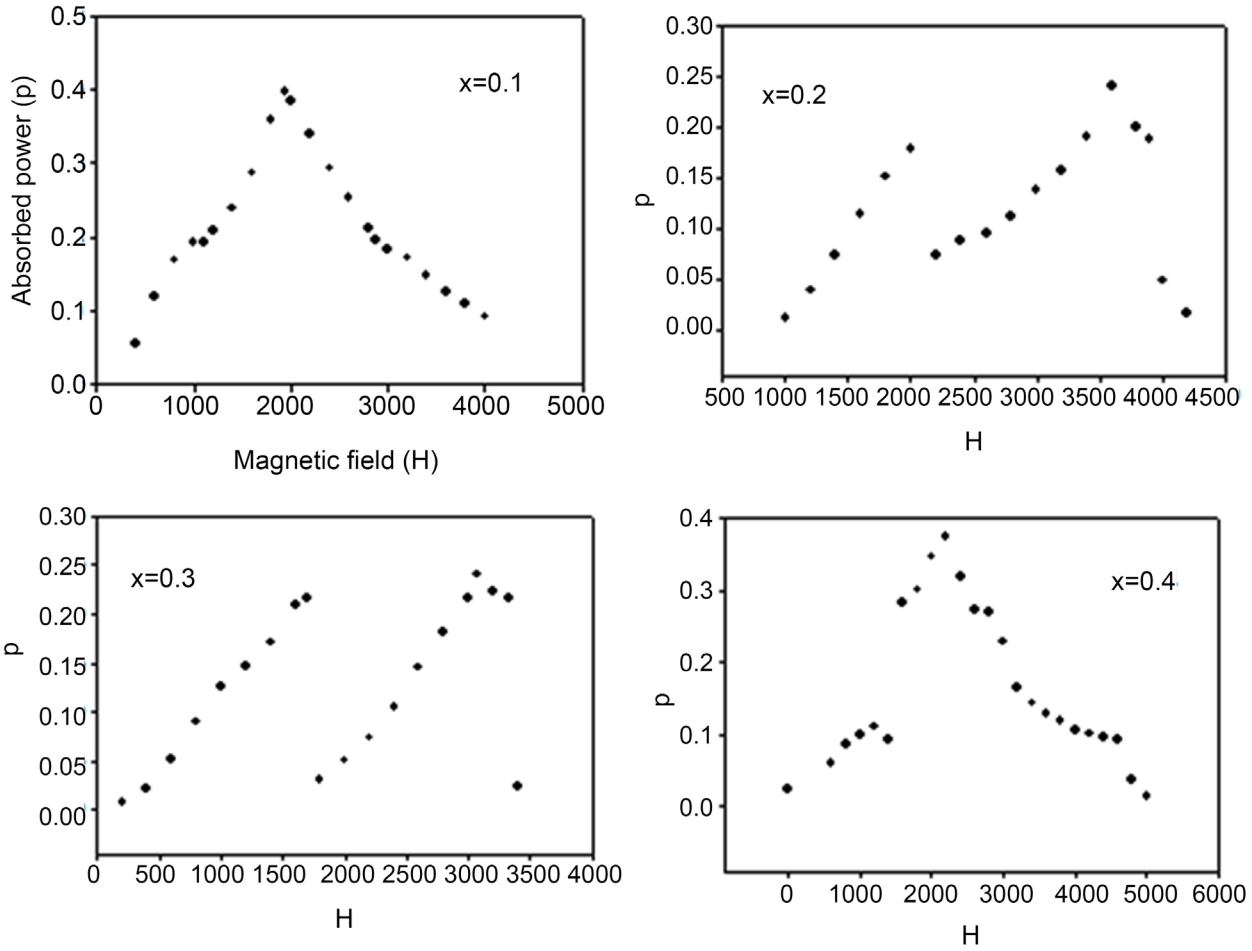

Figure 12. The variation of ESR absorption curves with compositions of the system $La_{1-x}Ho_xFeO_3$ ferrite.

Table 4. The line width of broadening ΔH, spectroscopic splitting factor (g) and the spin lattice relaxation process τ as a function of composition for $La_{1-x}Ho_xFeO_3$ ferrite.

x	ΔH	g_1	g_{11}	T
0.1	1028	6.38	2.44	$1.10e^{-15}$
0.2	1000	4.79	2.47	$1.70e^{-15}$
0.3	1166	5.63	2.89	$1.38e^{-15}$
0.4	1363	6.81	2.10	$5.82e^{-16}$

line width. The spin-spin relaxation time, which arises from the influence of one magnetic ion on another, limits the broadening of the line width. In this case spin-spin relaxation time increased with increasing Ho addition leading to the increase in the line width. The spin relaxation time is given by the following equation:

$$\tau = \frac{2\left(1.1\times10^{11}\right)}{g\Delta\beta_{pp}\sqrt{3}}$$

where g is the spectroscopic splitting factor and $\Delta\beta_{pp}$ is the separation between

the two peaks in ESR spectra.

3.5. Dielectric Constant (ϵ) of $La_{1-x}Ho_x FeO_3$ Ferrite

The dielectric relaxation process in ferrite can be identified with electron hopping among Fe^{2+} and Fe^{3+} sites with the arrangement of its different nearest neighbor either in the form of impurity band conduction or variable range hopping. The dielectric relaxation process occurs when the jumping frequency of localized electric charge carriers becomes nearly equal that of applied ac electric field. The dielectric constant of the system $La_{1-x}Ho_xFeO_3$ increases by increasing temperature as shown in Figure 13.

It is noticed that the dielectric constant (ϵ) decreases by increasing Ho content at 1 KHz. The electronic exchange interaction $Fe^{2+} \leftrightarrow Fe^{3+}$ gives local displacement of electrons in the direction of an applied electric field which induces polarization in ferrite. The formation of orthorhombic phase as a result of Ho addition decreases the conduction process between Fe^{2+} and Fe^{3+} leading to the decrease of electric polarization and hence the dielectric constant. The behavior of our results is similar to that in previous work [22].

Figure 14 shows the variation of tanδ (dielectric loss) as a function of temperature at different Ho content at 1 KHz. The slight increase was found till 170˚C above which the increase is much faster with increasing temperature. This can be illustrated to increase g the A.C. conductivity with rising temperature because the hopping rate of electrons between Fe^{3+} ions and Fe^{2+} are thermally activated. The behavior of our results is similar to that in previous work [22].

4. Conclusion

The X-ray diffraction analysis of the samples of the system $La_{1-x}Ho_xFeO_3$ ensures

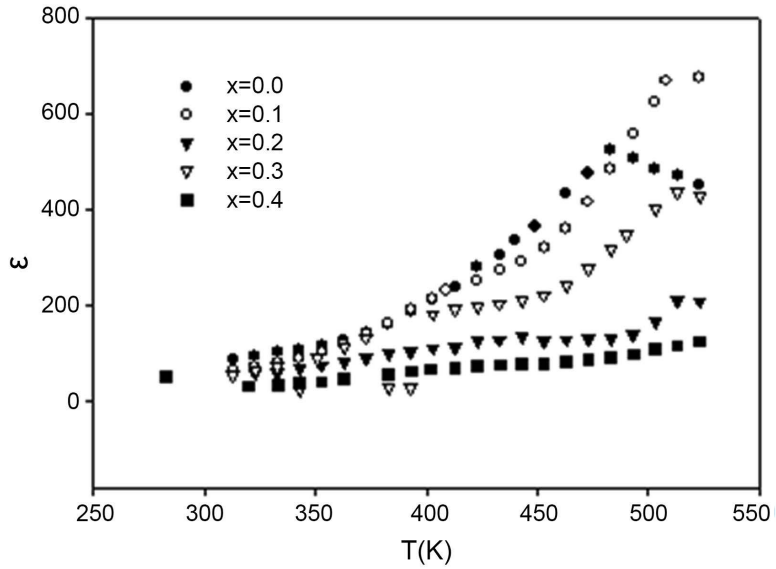

Figure 13. The dielectric constant (ϵ) of $La_{1-x}Ho_xFeO_3$ as a function of temperature T(K) at constant frequency 1 KHz.

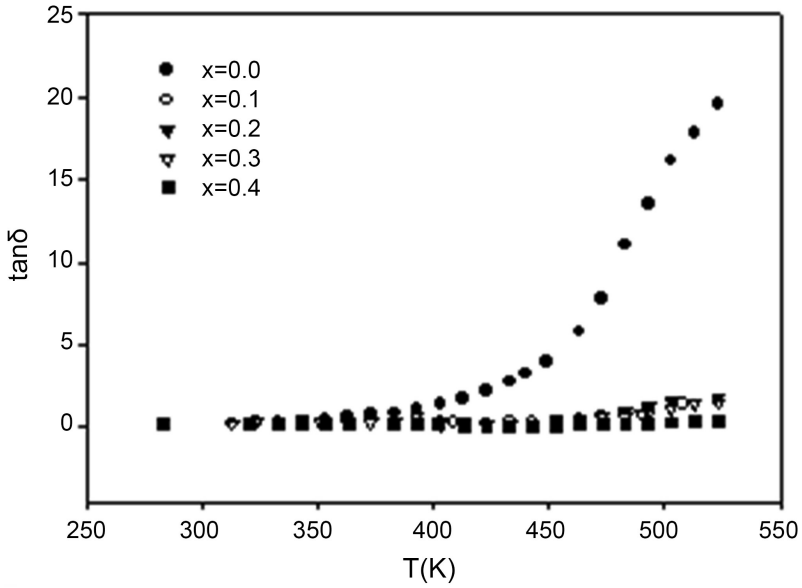

Figure 14. Dielectric loss as a function of temperature T(K) at different Ho content.

the orthorhombic-phase structure without any residuals of the original constituent oxides. The lattice parameters (a, b and c), the volume of the lattice (V), increase by increasing Ho content. The measured density is less than that predicted from X-ray measurements and the porosity increases by increasing Ho content. The DC electrical conductivity of the system $La_{1-x}Ho_xFeO_3$ increases linearly with increasing temperature which ensures the semiconducting nature of the samples and decreases with increasing Ho content. IR spectra of the system $La_{1-x}Ho_xFeO_3$ ferrite showed two main characteristic absorption bands in the far infrared region. For $x = 0.2$, 0.3 and 0.4, the ESR spectra deviate from Lorentzian shape and hyperfine interaction takes place between the first spinel phase and the second orthorhombic phase and two peaks appear. The X-ray diffraction patterns of $La_{1-x}Ho_xFeO_3$ indicate that all samples possess an orthorhombic structure. The dielectric constant of the composition $La_{1-x}Ho_xFeO_3$ ($x = 0.0$, 0.1, 0.2, 0.3 and 0.4) increases by increasing temperature and decreases by increasing Ho content.

Conflicts of Interest

The authors declare no conflicts of interest regarding the publication of this paper.

References

[1] Kanbe, S., Hasegaw, T., Aoki, M., Nakamura, T., Kishio, K., Kitazawa, K., Takagi, H., Uchida, S., Tanaka, S. and Fueki, K. (1987) High Tc Superconductivity in Tm-Ba-Cu-O System. *Japanese Journal of Applied Physics*, **5**, 613. https://doi.org/10.1143/JJAP.26.L613

[2] Stopples, D. (1982) Magnetic Permeability of Monocrystalline MnZn Ferrous Ferrite in a Simple Model Video Recording Head. *Journal of Magnetism and Magnetic*

Materials, **26**, 306.

[3] Forestier, H. and Guit-Guillain, G. (1950) A New Series of Ferromagnetic Bodies: the Ferrites of Rare Earths. *Comptes Rendus*, **230**, 1884.

[4] Geller, S. and Bala, V.B. (1956) Crystallographic Studies of Perovskite-Like Compounds. II. Rare Earth Alluminates. *Acta Crystallographica*, **9**, 1019-1025. https://doi.org/10.1107/S0365110X56002965

[5] White, R.L. (1969) Review of Recent Work on the Magnetic and Spectroscopic Properties of the Rare-Earth Orthoferrites. *Journal of Applied Physics*, **40**, 1061. https://doi.org/10.1063/1.1657530

[6] Cashion, J.D., Cooke, A.H., Martin, D.M. and Wells, M.R. ((1970) Magnetic Properties of Gadolinium Ortho-Aluminate. University of Oxford, Oxford.

[7] Chu, N.J., Wang, X.Q., Liu, Y.P., Jin, H.X., Wu, Q., Li, L., Wang, Z. and Ge, H.L. (2009) Magnetic Properties of Low Mn-Doped NiCuZn Nanocrystalline Ferrites. *Journal of Alloys and Compounds*, **470**, 438-442. https://doi.org/10.1016/j.jallcom.2008.02.095

[8] Geller, S. and Wood, E. (1956) Crystallographic Studies of Perovskite-Like Compounds. I. Rare Earth Orthoferrites and $YFeO_3$, $YCrO_3$, $YAlO_3$. *Acta Crystallographica*, **9**, 563. https://doi.org/10.1107/S0365110X56001571

[9] Goldschmidt, V.M. (1926) Die Gesetze der Krystallochemie. *Naturwissensenschaffen*, **14**, 477-485. https://doi.org/10.1007/BF01507527

[10] Dong, C. (1999) A Windows-95-Based Program for Powder X-Ray Diffraction Data Processing. *Powder X Applied Crystallography* (*Copenhagem*), **32**, 838. https://doi.org/10.1107/S0021889899003039

[11] Li, K., Li, X., Zhu, K., Zha, J. and Zhang, Y. (1997) Growth, Structural Characteristics and Magnetoresistance in LaCaMnO Thin Films Prepared by DC Magnetron Sputtering. *Journal of Applied Physics*, **81**, 6943.

[12] Gienier, J.C., Pouch, M. and Hogenmuller, P. (1977) Caracterisations physiques du ferrite de plomb $Pb_2Fe_2O_5$. *Reviews in Chemistry of Minerals*, **14**, 515.

[13] Dwcrus, J.C., Maln, O.G. and Thomson, A.W. (1963) Modern Trends in Physics. *Proceedings of the Royal Society A*, **275**, 295.

[14] Rezlescu, E., Rezlescu, N., Popa, P.D., Rezlescu, L. and Pasnicu, C. (1997) The Influence of R_2O_3 (R = Yb, Er, Dy, Tb, Gd, Sm and Ce) on the Electric and Mechanical Properties of a Nickel-Zinc Ferrite. *Physica Status Solidi* (*A*), **162**, 673. https://doi.org/10.1002/1521-396X(199708)162:2<673::AID-PSSA673>3.0.CO;2-A

[15] Hemeda, O.M., Barakat, M.M. and Hemeda, D.M. (2004) Structural, Electrical and Spectral Studies on Double Rare-Earth Orthoferrites $La_{1-x}Nd_xFeO_3$. *Turkish Journal of Physics*, **27**, 537-550.

[16] Hemeda, O.M., Mahmoud, K.R. and Sharshar, T. (2014) Structure, Electric Properties and Positron Annihilation Studies of $CuZnFe_2O_4$ Doped with $BaTiO_3$. *The European Physical Journal Plus*, **129**, 173.

[17] Hemeda, O.M. (2002) Electron Spin Resonance and Cation Distribution Studies of the $Co_{0.6}Zn_{0.4}MnxFe_{2-x}O_4$ Ferrite System. *Journal of Magnetism and Magnetic Materials*, **251**, 50-60. https://doi.org/10.1016/S0304-8853(02)00451-1

[18] Hemeda, O.M., Mahmoud, K.R., Sharshar, T., Elsheshtawy, M. and Hamad, M.A. (2003) ESR, Thermoelectrical and Positron Annihilation Doppler Broadening Studies of $CuZnFe_2O_4$-$BaTiO_3$ Composite. *Journal of Magnetism and Magnetic Materials*, **429**, 124-128. https://doi.org/10.1016/j.jmmm.2017.01.018

[19] Byeon, S.C. and Hong, K.S. (1998) Line Width of Manganese-Zinc Ferrite Poly-

crystals with Oxygen Partial Pressure. *Journal of Applied Physics*, **83**, 432. https://doi.org/10.1063/1.367829

[20] Galt, J.K. (1954) Motion of Individual Domain Walls in a Nickel-Iron Ferrite. *Bell System Technical Journal*, **33**, 1023. https://doi.org/10.1002/j.1538-7305.1954.tb02363.x

[21] Clogston, A.M. (1955) Relaxation Phenomena in Ferrites. *Bell System Technical Journal*, **34**, 739. https://doi.org/10.1002/j.1538-7305.1955.tb03774.x

[22] Olofa, S.A., Tawfik, A., Barakat, M.M. and Mosaad, M.M. (1991) Thermal Conductivity of the Ferrites $Ni_{0.65}Zn_{0.35}Cu_xFe_{2-x}O_4$. *Journal of Thermal Analysis*, **37**, 2277-2284. https://doi.org/10.1007/BF01913727